LS-MERGE: MERGING LANGUAGE MODELS IN LATENT SPACE

Anonymous authors
Paper under double-blind review

ABSTRACT

Model merging in weight space is an efficient way to reuse pretrained models, but existing methods typically assume matching architectures or sizes, making heterogeneous merges brittle or infeasible. We address this limitation by encoding model weights into a smooth latent space, enabling cross-architecture operations, and performing the merge in the latent space before decoding back to weights. This approach faces two major challenges. First, LLMs contain billions of parameters, which makes latent encoding computationally demanding. Second, using high compression ratios often hinders the encoder's ability to generalize to unseen weights. We tackle these issues with a transformer-based variational autoencoder (VAE) trained in a two-stage compression curriculum with structured layer-aware chunking: the model first learns a high-capacity latent representation and then distills to a compact code, improving both stability and out-of-distribution generalization. To align heterogeneous models, we introduce a dimensionality-matching projection that allows interpolation between models of different sizes. Empirically, latent-space interpolation is consistently more robust than direct weight-space averaging and yields stronger downstream performance when merging models of different sizes. Together, these components provide a scalable, architecture-agnostic recipe for model merging.

1 INTRODUCTION

Large Language Models (LLMs) are foundational to modern artificial intelligence. However, their pretraining demands millions of GPU-hours, leading to a significant inefficiency if the acquired knowledge remains confined to a single model instance. To mitigate this cost and enhance utility, weight-space model merging has emerged as a promising approach. This technique combines parameters from multiple pretrained models to integrate complementary capabilities and improve performance on diverse tasks, all without additional pretraining (Yang et al., 2024).

Existing merging methodologies range from straightforward linear interpolation (Wortsman et al., 2022) to sophisticated evolutionary search-based fusion (Akiba et al., 2025), consistently demonstrating practical benefits at scale. Despite these advancements, current techniques typically face two significant limitations: (i) Requirement for multiple source models: Most approaches necessitate at least two distinct pretrained models for merging, which restricts their application when the goal is to enhance or adapt a single existing model. (ii) Architectural homogeneity: Merging methods frequently assume shape-compatible or architecturally homogeneous models, hindering their use with mismatched architectures (e.g., varying widths or depths) (Yu et al., 2024a). These constraints significantly limit the broad applicability of merging across diverse LLM checkpoints as well as self-merging. Addressing these constraints is crucial for unlocking the full potential of pretrained LLM checkpoints and fostering a more flexible and efficient paradigm for model reuse.

Recent advancements in weight-space learning (Sch"urholt et al., 2024) offer a compelling opportunity to overcome the aforementioned limitations in LLM merging. These approaches operate directly on pretrained model weights as the input data modality. By projecting parameters from diverse models into a smooth, unified latent space of consistent dimensionality, we can inherently mitigate the challenge of architectural mismatch. Specifically, these parameter signals can be embedded into identical-dimensionality representations using powerful generative models such as Variational Autoencoders (VAEs) (Kingma & Welling, 2013), normalizing flows (Kobyzev et al., 2021), or

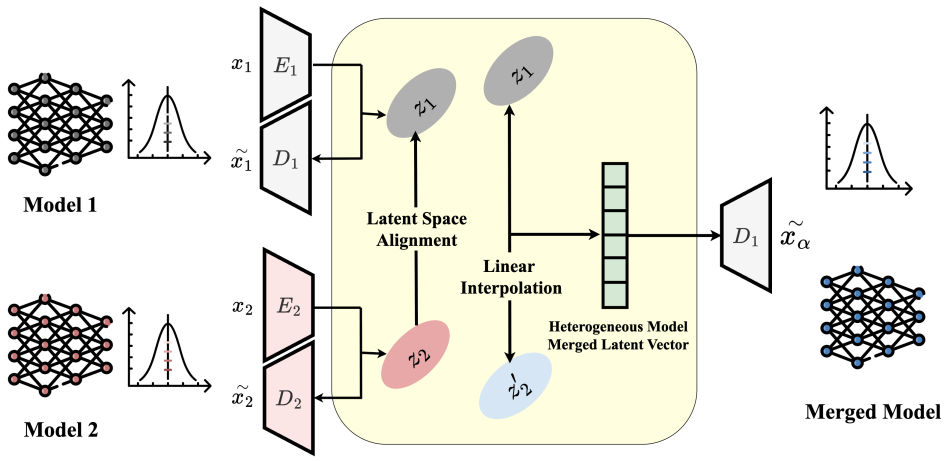

Figure 1: **LS-Merge: encode, align, and decode for LLM weight merging.** **(a)** Pretrained weight tensors x_1 and x_2 are chunked layer-wise and encoded by E_1, E_2 into latents z_1, z_2; decoders D_1, D_2 reconstruct $\tilde{x}_1, \tilde{x}_2$. **(b)** A latent-space alignment places z_1 and z_2 in a shared manifold where they are merged(linear interpolation) yielding a merged latent z_α, supporting both homogeneous (same-architecture(same encoding model) and heterogeneous (cross-architecture) merges. **(c)** A target decoder (e.g., D_1) maps z_α back to weights $\tilde{x}_\alpha$, producing the merged model. Here, x_i denotes the full weight set of model i, z_i its latent code, and tildes indicate reconstructions.

diffusion models (Wang et al., 2025). While these innovative latent-space methods have demonstrated considerable success in vision and other domains, their application to the encoding and subsequent merging of pretrained LLM weights remains a largely unexplored frontier.

We propose LS-Merge, a novel framework that fundamentally shifts the merging process from the raw weight space to a learned latent space. This paradigm enables both homogeneous and heterogeneous merging by design: (i) Enabling single-model augmentation: A generative model can learn the latent manifold of a single LLM parameters, facilitating "merging" operations within this latent space. This allows for the exploration of variations, specializations, or the enhancement of capabilities derived solely from the original model, obviating the need for an external second model. (ii) Facilitating heterogeneous integration: By projecting diverse LLM architectures into a common, fixed-dimensional latent space, the stringent constraints of architectural homogeneity are significantly relaxed. Merging operations then occur within this unified latent representation, enabling the seamless integration of knowledge from models with differing widths, depths, or even fundamental architectural designs, as our method operates solely on the tensor data within the latent space. In summary, LS-Merge advances LLM merging through the following key contributions:

- **Weight statistics that matter for encoding.** We show that LLM weights exhibit low variance with heavy tails, that could significantly affect the choice of encoding network.
- **Merging LLMs in latent space.** We propose LS-Merge, a novel latent-space merging methodology that enables merging LLMs in their weights latent space.
- **Heterogeneous merging.** We introduce a dimensionality-matching projection and OT-based latent alignment that enables interpolation between models of different depths or widths.
- **Consistent empirical gains.** On Gemma and LLaMA pretrained models and LoRA-experts merging, our latent space merging method outperforms existing merging methods and remains robust under heterogeneity.

2 Related Work

Model averaging The simplest merging approach directly averages weights. Model Soup (Wortsman et al., 2022) showed that averaging fine-tuned checkpoints from the same initialization improves

generalization. Extensions include Uniform Soup (Wortsman et al., 2022) for LoRA weights and spherical linear interpolation (SLERP), which interpolates on the unit hypersphere but remains a pairwise-only method that merges only two models at a time and requires identical architectures.

Interference-aware techniques Merging models from different tasks can cause misalignment. Yadav et al. (2023) uses trimming and sign alignment, Yu et al. (2024a) sparsifies and rescales fine-tuned deltas, and Yu et al. (2024b) combine both. Greedy Soup (Wortsman et al., 2022) and EvolMerge (Akiba et al., 2025) treat merging as an optimization problem, while Task Arithmetic (Ilharco et al., 2023) models task vectors in parameter space. These methods require aligned architectures and incur computational cost.

Modular assembly Instead of merging weights, some approaches combine modules or experts. Model Stocks (Jang et al., 2024) and LoraHub (Huang et al., 2023) aligns LoRA adapters, Pack of LLMs (Mavromatis et al., 2024) learns expert routing, and cBTM (Gururangan et al., 2023) merges task-specific experts via unsupervised domain discovery. Modular systems are flexible but increase inference cost and do not unify knowledge into a single parameter set.

All prior methods operate in weight or module space and assume architectural alignment. In contrast, we propose **latent-space model merging**, which generalizes beyond these constraints.

3 LS MERGE

We present **LS-Merge**, a framework for performing model merging *in latent space*. As illustrated in Figure 1, we encode pretrained LLM weights, operate on their latent representations (including alignment when heterogeneous), and decode back to parameters to obtain the merged model.

3.1 EXPLORING WEIGHT DYNAMICS IN LLMS

To motivate our design, we analyze the distributional properties of transformer submodules in Gemma-3 (Team et al., 2025) and LLaMA-3.2 (Grattafiori et al., 2024). We compute the first four moments (mean, variance, skewness, and kurtosis) for self-attention layers (q_proj, k_proj, and o_proj) and MLP layers (up_proj, down_proj, and gate_proj). Table 1 reports the statics stands for per moment with full details in appendix Table 9. Weights exhibit near-zero means, low variances, and small positive skewness, but *markedly high kurtosis* in earlier layers, especially in self-attention projections. High kurtosis, i.e., leptokurtic distributions, indicates sharp peaks with heavy tails: rare, large-magnitude parameters that are likely functionally important. This contradicts Gaussian assumptions used in prior work (Si et al., 2025) and suggests that encoders must preserve tail events rather than over-regularize toward a narrow Gaussian. We observe this pattern consistently across sizes within both families.

Theoretical Compressibility of LLM Weights As the LLM weights distribution shows heavy tails and low intrinsic variance, we investigate whether a simple VAE can compress LLM weights effectively. Let $W \in \mathbb{R}^{n\times m}$ be a layer matrix and let $w = \mathrm{vec}_{\mathrm{row}}(W) \in \mathbb{R}^D$ denote the row-wise concatenation (flattening) of W with $D = nm$. Empirically (Fig. 2), the top $r \ll \min(n, m)$ principal components capture nearly all variance, i.e., $\sum_{i=1}^{r} \lambda_i / \sum_{i=1}^{D} \lambda_i \approx 1$, where $\{\lambda_i\}$ are the eigenvalues of the empirical covariance of w (equivalently, proportional to squared singular values of W). By Eckart–Young theorem (Eckart & Young, 1936), the best rank-r approximation W_r satisfies $\|W - W_r\|_F^2 = \sum_{i>r} \lambda_i$ and can be stored with $O(r(n + m))$ parameters (e.g., $U_r \in \mathbb{R}^{n\times r}$, $V_r \in \mathbb{R}^{m\times r}$). Thus, weights concentrate near a low-dimensional set. Assuming the collection of flattened weights $\mathcal{W} \subset \mathbb{R}^D$ concentrates near a smooth d-dimensional manifold $\mathcal{M}$ with $d \ll D$, manifold embedding results (Bengio et al., 2012; Lahiri et al., 2016) imply the existence of $\Phi : \mathbb{R}^D \to \mathbb{R}^k$ with $k = O\big(\frac{d}{\varepsilon^2} \log \frac{V}{\tau}\big) \ll D$ that preserves pairwise distances on $\mathcal{M}$ within $(1 \pm \varepsilon)$, where V bounds manifold volume and τ its reach. This confirms that there exists a projection map to a lower dimension which can be approximated by an encoder A VAE encoder $f_\theta : \mathbb{R}^D \to \mathbb{R}^k$ with decoder $g_\phi : \mathbb{R}^k \to \mathbb{R}^D$ can approximate such compressive embeddings while modeling uncertainty, justifying our latent compression.

layers	llama3-2-3b-it				gemma-3-1b-it				gemma-3-4b-it			
	mean	var.	skew	kurt.	mean	var.	skew	kurt.	mean	var.	skew	kurt.
self_attn	0	0.0017	0.0192	8.4032	0.0002	0.0031	0.0500	15.0505	0	0.0015	0.0501	15.2010
	0	0.0013	0.0191	7.3438	0.0002	0.0030	0.0450	9.8347	0	0.0015	0.0267	7.3832
	0	0.0012	0.0178	6.2172	0.0001	0.0030	0.0389	9.0363	0	0.0014	0.0255	7.2277
	0	0.0011	0.0104	5.4477	0.0001	0.0030	0.0288	8.6496	0	0.0014	0.0172	6.0731
avg (self_attn)	0	0.0005	-0.0002	1.4342	0	0.0012	-0.0009	3.2858	0	0.0005	0.0009	2.6900
mlp	0	0.0005	0.0093	5.4740	0.0002	0.0010	0.0167	8.7665	0	0.0004	0.0266	6.3297
	0	0.0005	0.0080	4.1465	0.0002	0.0010	0.0090	3.1514	0	0.0004	0.0155	5.9670
	0	0.0004	0.0075	2.6694	0.0002	0.0010	0.0077	3.0577	0	0.0004	0.0130	2.7454
	0	0.0004	0.0074	2.4364	0.0002	0.0010	0.0071	3.0113	0	0.0004	0.0094	2.4371
avg (mlp)	0	0.0003	0.0003	0.8435	0	0.0006	0	1.1739	0	0.0003	0.0006	1.0807

Table 1: Layer-wise distribution statistics of model parameters for three instruction-tuned LLMs: **llama3-2-3b-it**, **gemma-3-1b-it**, and **gemma-3-4b-it**. For each model and block type (`self_attn` and `mlp`), we report the first four moments of the flattened weight tensors: *mean*, *variance*, *skewness*, and *excess kurtosis*. Per-row entries list representative layers in each block; the `avg` row aggregates across all layers for that block and model. Means are near zero and variances are small, while skewness and especially kurtosis (often > 5 and up to ~ 15) indicate pronounced heavy tails and asymmetry. These non-Gaussian, heavy-tailed statistics motivate encoders that preserve rare but high-magnitude outliers.

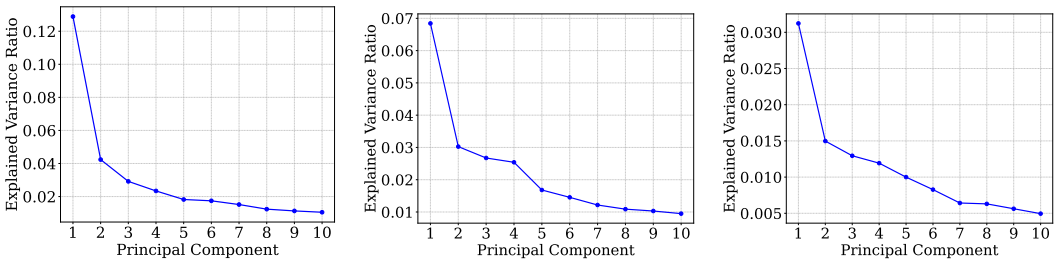

(a) Llama3-2-3b-it layer 0 k_proj (b) Gemma-3-1b-it layer 0 k_proj (c) Gemma-3-4b-it layer 0 k_proj

Figure 2: Plots of the PCA **explained-variance ratio** for first k projection weight matrices per model from three LLM checkpoints: Llama-3-2-3b-it, Gemma-3-1b-it, and Gemma-3-4b-it. Additional results are reported in the appendix A. For each model, we show the four projection matrices of self-attention (*q, k, v, o*). The sharp drop after the leading principal components highlights a low-rank structure that is consistent across architectures and model sizes.

3.2 LLM Weights Preprocessing and Encoding

We first standardize pretrained LLM weights of varying shapes and store the normalized tensors offline. We then learn a compact latent representation with a transformer-based VAE, chosen for its strong generalization to unseen checkpoints and faster training than convolutional alternatives at a comparable parameter count.

Preprocessing as a Sequence For each layer, we flatten its weight tensor to $w \in \mathbb{R}^L$, then zero-pad to $L_p = \lceil L/c \rceil \, c$ and partition into $n = L_p/c$ non-overlapping chunks $\{c_i\}_{i=1}^n$ of size c. A batch becomes $X \in \mathbb{R}^{B \times n \times c}$. Each chunk is embedded to $X_{\text{emb}} \in \mathbb{R}^{B \times n \times d}$ and passed through a transformer encoder E_θ with optional token downsampling. The latent is

$$z = E_\theta(X_{\text{emb}}) \in \begin{cases} \mathbb{R}^{B \times z_d} & \text{(pooled over tokens)} \\ \mathbb{R}^{B \times n \times z_d} & \text{(token-wise)} \end{cases}$$

The decoder D_ϕ is trained to reconstruct chunked weights from the latent z. We optimize the β-VAE objective in eq. 1

$$\mathcal{L} \;=\; -\,\mathbb{E}_{q_\phi(z \mid w)}\big[\log p_\theta(w \mid z)\big] \;+\; \beta\,\mathrm{KL}(q_\phi(z \mid w) \,\|\, p(z))\,, \tag{1}$$

with $p(z)$ standard Gaussian and fixed β.

Stabilizing Training on Heavy-Tailed Weights Since LLM weights distribution has low variance and heavy tails (Section 3.1; Appendix 5), training VAEs on these weights can lead to collapse in the early training stage. We use (i) transformer blocks (Vaswani et al., 2017) in E_θ, D_ϕ for long-range coupling across chunks and (ii) a two-stage curriculum: first train a deterministic autoencoder (KL off) to convergence, then enable the KL term and fine-tune to structure the latent space without sacrificing fidelity. The VAE performance is measured by the performance of the reconstructed weights when used to initialize the corresponding architectures.

3.3 Latent Space Alignment and Merging

Self-Merging and Homogeneous Merging *Self-merging* encodes a single model and draws multiple latent codes from its posterior (or the prior) to combine them, which is equivalent to merging *homogeneous* models whose per-layer embeddings share the same dimensionality. To be specific, for two checkpoints with weights $W_a, W_b \in \mathbb{R}^N$, we encode $z_a = E(W_a)$ and $z_b = E(W_b)$, and linearly interpolate them as $z_\lambda = (1-\lambda)z_a + \lambda z_b$ for $\lambda \in [0,1]$. We obtain the weights by decoding the interpolated latent $\widehat{W}_\lambda = D(z_\lambda)$. Empirically, latent-domain interpolation better preserves functional coherence than direct weight-space mixing, and common merge operators, for example, model soup or task arithmetic (Wortsman et al., 2022; Ilharco et al., 2023), transfer naturally by applying them to $\{z_a, z_b\}$ before decoding.

Heterogeneous Mapping (depth/width mismatch) When two architectures match, layer by layer, in the number of weight chunks, we employ a single VAE to embed all layers into a common d-dimensional latent space. If the per-layer number and chunk counts differ, we instead deploy separate encoders for each architecture. Let the source have n_s layers with size M, and the target n_t layers with size N. We embed per-layer latents to a fixed dimension d and rescale the source so that total capacity matches the target:

$$r = \frac{n_t\, N}{n_s\, M}, \quad Z^{(\text{src, mapped})} \in \mathbb{R}^{n_t \times d}, \quad Z^{(\text{tgt})} \in \mathbb{R}^{n_t \times d}.$$

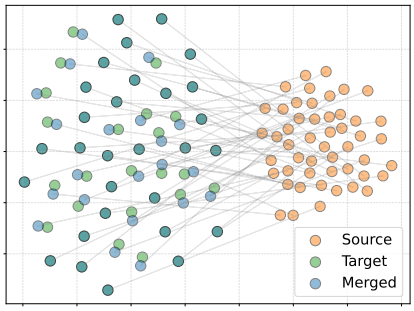

Figure 3: Visualization of embeddings of Gemma models and OT-aligned latents. The merged latent is partially overlapped with the target latent.

This proportional alignment across depth and width standardizes each architecture to a common per-layer latent dimensionality, enabling interpolation and the use of standard merge operators. However, when VAEs are trained separately per architecture (or under different training regimes), their *latent distributions* can differ, so equal shape does not guarantee comparability.

Optimal Transport Alignment. While latent encoding standardizes per-layer dimensionality, it does not guarantee that two models' latent representations are geometrically compatible. As shown in Appendix C (Figure 9a), homogeneous models (e.g., checkpoints from the same pre-training run) exhibit overlapping latent support and often satisfy *Linear Mode Connectivity*, making linear interpolation well-behaved. In contrast, heterogeneous models such as Gemma and Llama produce latent distributions $\mathcal{Z}_{\text{src}}, \quad \mathcal{Z}_{\text{tgt}}$ that lie on disjoint manifolds with different covariance structures and density profiles (Figure. 9b). Interpolating between such misaligned latents could produce low performing weights that fall outside the target decoder's valid manifold and degrade functionality(performance on down stream tasks). To address this, we treat heterogeneous merging as a *manifold registration* problem and align the source latent distribution to the target using Optimal Transport (OT) (Villani, 2009; Santambrogio, 2015). OT provides a principled framework for finding a map $T : \mathcal{Z}_{\text{src}} \to \mathcal{Z}_{\text{tgt}}$ that minimizes geometric distortion while reshaping one distribution into the other. Formally, we solve the Monge problem under the 2-Wasserstein distance 2:

$$T^* = \arg\min_T \int \|z - T(z)\|_2^2 \, d\mu_{\text{src}}(z) \quad \text{s.t.} \quad T_{\#}\mu_{\text{src}} = \mu_{\text{tgt}}, \tag{2}$$

where $T_{\#}\mu_{\text{src}}$ denotes the pushforward measure induced by T. This ensures that applying T^* to source latents produces samples distributed as the target. While the general Monge problem is

Algorithm 1 Heterogeneous LLM Parameter Merging in Latent Space

Require: Source weights W_{src}, target weights W_{tgt}, encoder–decoder (E, D)
Ensure: Merged weights W_{merged}

1: Extract per-layer groups $L_{\text{src}}, L_{\text{tgt}}$; set $N \leftarrow \min(|L_{\text{src}}|, |L_{\text{tgt}}|)$ and define pairs $(l_{\text{src}}^{(j)}, l_{\text{tgt}}^{(j)})_{j=1}^{N}$
2: **for** $j = 1$ to N **do**
3: Flatten & chunk $w_{\text{src}}^{(j)}, w_{\text{tgt}}^{(j)}$; encode $z_{\text{src}}^{(j)} \leftarrow E(w_{\text{src}}^{(j)})$, $z_{\text{tgt}}^{(j)} \leftarrow E(w_{\text{tgt}}^{(j)})$
4: Proportional mapping to fixed d: obtain $Z_{\text{src}}^{(j)}, Z_{\text{tgt}}^{(j)} \in \mathbb{R}^{n_t \times d}$
5: OT alignment: $\tilde{Z}_{\text{src}}^{(j)} \leftarrow \text{OT-ALIGN}\left(Z_{\text{src}}^{(j)}, Z_{\text{tgt}}^{(j)}\right)$ (solve equation **??**)
6: Interpolate latents: $Z_{\lambda}^{(j)} \leftarrow (1-\lambda)\, Z_{\text{tgt}}^{(j)} + \lambda\, \tilde{Z}_{\text{src}}^{(j)}$
7: Decode & assemble: $w_{\text{merged}}^{(j)} \leftarrow D\left(Z_{\lambda}^{(j)}\right)$; place into W_{merged}
8: **end for**
9: **return** W_{merged}

computationally intensive, can approximate each layer's latent distribution as a high-dimensional Gaussian defined by its empirical mean μ_s and covariance Σ_s. Under this assumption (**?**), the optimal transport map admits a closed-form affine solution: $\tilde{z}_{\text{src}} = T^*(z_{\text{src}}) = \mu_t + A\,(z_{\text{src}} - \mu_s)$, where $A = \Sigma_s^{-1/2}\left(\Sigma_s^{1/2}\,\Sigma_t\,\Sigma_s^{1/2}\right)^{1/2}\Sigma_s^{-1/2}$. This transformation aligns both the mean and covariance of the source latents to the target, effectively registering the two manifolds and removing the geometric mismatch. In practice, we use existing OT library from Flamary et al. (2021; 2024) in our work.

After alignment, the transported latents $\tilde{Z}_{\text{src}}$ and the target latents Z_{tgt} share a common support, and we perform interpolation in this aligned space: $Z_{\lambda}^{\text{OT}} = (1-\lambda)\, Z_{\text{tgt}} + \lambda\, \tilde{Z}_{\text{src}}$. Because Z_{λ}^{OT} now lies within the target decoder's valid density region (Agustsson et al., 2019), the decoded weights remain stable and functional, enabling robust cross-architecture merging even between disparate model families. The overall process for heterogeneous LLMs merging is summarized in algorithm 2.

4 Experiments

General Setup We evaluate latent–space merging on `Gemma-3-1B-it`, `Gemma-3-4B-it`, `Llama-3-1B-instruct`, `Llama-2-7b`, and benchmark latent–space expert fusion against weight–space merging using 10 LoRA experts on `Gemma-7B-it`.

Datasets and Tasks We first use subset dataset used by Feng et al. (2024b), such as language understanding (MMLU (Hendrycks et al., 2021), MMLU-pro (Wang et al., 2024b)), commonsense reasoning (HellaSwag (Zellers et al., 2019)), math (GSM8k (Cobbe et al., 2021)), and knowledge-intensive tasks (Knowledge Crosswords (Ding et al., 2024), NLGraph (Wang et al., 2024a), TruthfulQA (Lin et al., 2022), AbstainQA (Feng et al., 2024a)).

Training data consist of pretrained weight snapshots for `Gemma-3-1B-it` and `Gemma-3-4B-it`, plus LoRA experts from Feng et al. (2024b).

Baselines We compare against reference-free weight–space methods: spherical linear interpolation (SLERP), uniform soup (Wortsman et al., 2022), greedy soup (Wortsman et al., 2022), data-level merging, the raw pretrained checkpoints, and the best single expert per task. This excludes approaches that require access to an unmodified base reference model.

Evaluation Protocols We evaluate compression and merging in four scenarios:

1. **Self-Merging:** sample multiple codes from one model's latent distribution and merge them.
2. **Expert Merging:** merge LoRA experts in latent space vs. weight space.
3. **Cross-Architecture Merging:** align and merge models with various depths and widths.
4. **Ablation study:** reconstruction or compression behavior and generalization to unseen checkpoints.

	MMLU	MMLU-pro	HellaSwag	Gsm8k
Gemma-3-4b-it	53.10	20.90	47.40	29.90
VAE	54.10 ± 0.36	20.80 ± 0.20	49.03 ± 0.70	31.27 ± 0.55
LS-Merge	**54.20 ± 0.00**	**21.02 ± 0.03**	**50.10 ± 0.00**	**32.20 ± 0.05**
Gemma-3-1b-it	32.20	7.10	28.70	16.90
VAE	32.60 ± 0.26	7.60 ± 0.56	28.57 ± 0.12	16.77 ± 0.12
LS-Merge	**35.13 ± 0.02**	**10.30 ± 0.20**	**31.16 ± 0.14**	**17.50 ± 0.01**

Table 2: Benchmark scores for pretrained model, VAE, and LS-Merge.

	MMLU	MMLU-pro	HellaSwag	Gsm8k	TruthfulQA	NLGraph	K-Crossword	AbstainQA
Best expert	45.7	14.3	46.6	26.1	32.4	51.7	32.7	-10.8
Base model	48.8	18.1	53.3	6.9	30.1	47.5	28.0	-0.9
Data Merge*	44.5	17.6	52.7	14.3	10.7	42.3	**37.0**	-2.5
Uniform Soup	49.7	19.4	54.0	7.9	31.2	47.5	29.6	-0.1
SLERP(t=0.45)	52.5	18.8	50.4	25.5	28.7	49.8	30.0	-0.2
Greedy Soup	50.8	22.1	54.6	23.9	31.9	52.9	28.0	3.3
Dare-Ties	49.1	18.8	53.7	7.3	28.2	52.8	29.0	1.4
LS-Merge(lerp)	54.7	21.6	58.1	**28.1**	**33.0**	53.1	35.6	2.0
LS-Merge(soup)	**56.0**	**22.2**	**60.1**	24.2	32.0	**56.1**	35.2	**4.0**

Table 3: Results on merging expert LoRA weights in the raw weight space and the latent space.

Weight-Encoding Models We evaluated a Transformer-VAE and a ConvNet-VAE (Soro et al., 2025). We used AdamW (lr $= 1e{-}4$, weight decay $= 1e{-}5$) with a cosine-to-zero schedule. The checkpoints are from Hugging Face, and further details are given in the supplement. The learning rate was chosen on the basis of hyperparameter tuning.

4.1 Self-Merging for Enhanced Performance

We investigated a self-merging technique designed to enhance a single model's performance by exploring its learned latent distribution. The process involves encoding a model, sampling multiple latent codes from its posterior distribution, merging these codes into a single representation, and decoding it back into the parameter space. For this experiment, we used a single Transformer-VAE with six encoder and decoder blocks, trained jointly on weights from both `Gemma-3-1B-it` and `Gemma-3-4B-it` with the compression ratio held constant at 2. As shown in Table 2, this approach yields an average performance improvement of $\approx 4\%$ over two key baselines: the original base model and a standard VAE reconstruction from a single latent sample. Notably, the gains are more pronounced on the smaller model, consistent with it having tighter capacity constraints.

4.2 Merging LLM Experts in Latent Space

Next, we evaluated the primary application of our work: combining specialized LoRA experts. We compared our latent space approach against traditional weight-space interpolation methods using the experts from Feng et al. (2024b). In our method, each expert is encoded, their latent representations are merged, and then the resulting latent vector will be decoded into a single fused model. As shown in Table 3, our latent-space fusion consistently outperforms all weight-space baselines, including both linear and SLERP interpolation across uniform and greedy soup. We found this advantage stems from increased robustness. For example, greedy soup is highly sensitive to initialization, the checkpoint with the best validation accuracy often fails to yield the best test performance. By sampling multiple latent codes for each expert before merging, our method explores the learned parameter distribution instead of relying on a single point estimate, creating more robust and effective combinations.

4.3 Comparison to Representation-Merging Methods

To assess the robustness of our latent space approach, we benchmark it against leading representation-merging methods: Task Arithmetic (Ilharco et al., 2023) and Activation-Informed Merging (AIM) (Nobari et al., 2025), which operate on model activations rather than parameters. contrairily to the previous experiments, in this setting we use *lm-eval* tool (Gao et al., 2024) for fair comparison with the baselines. For this comparison, we merged `Llama-2-13B` models fine-tuned on distinct domains, utilizing a single VAE trained on the combined weights of all constituent models. The results

Method	MMLU	IFEval	MBPP	HumanEval	GSM8k
base	52.18	25.10	27.80	17.07	4.20
code	52.91	26.25	31.60	17.07	24.10
instruct	53.41	35.67	34.80	26.83	43.40
code + instruct (Task Arithmetic)	52.18	25.10	34.40	26.83	4.20
code + instruct (AIM)	54.18	32.00	36.00	**29.27**	**46.20**
code + instruct (LS-merge)	**55.07**	**36.41**	**36.02**	28.14	44.12

Table 4: Comparison of our latent space merging (LS-merge) with Task Arithmetic and AIM on `Llama-2-13B` fine-tuned models.

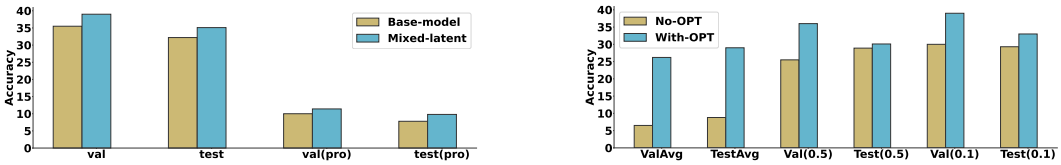

(a) Heterogeneous latent space merging.

(b) Varying coefficient on MMLU.

Figure 4: (a) Accuracy gains obtained by latent space merging of `Gemma-3-4B-it` with `Gemma-3-1B-it`. Bars show performance on the validation (*val*) and test splits of the MMLU and MMLU-PRO benchmarks (b) Impact of the merging coefficient t on validation and test accuracy in latent-space merging.

presented in Table 4 demonstrate that our method is highly competitive. It achieves performance comparable to the state-of-the-art AIM and substantially outperforms Task Arithmetic. This finding is significant, as it shows that a latent weight-space approach can match the performance of prominent methods that require access to model activations.

4.4 Cross-Architecture Merging

Our latent-space approach supports merging across substantial architectural gaps. We study two settings: (i) *intra-family* (different sizes within Gemma) and (ii) *cross-family* (Gemma $\leftrightarrow$ LLaMA).

Intra-family (Gemma-3-4B-it $\rightarrow$ Gemma-3-1B-it). Direct latent interpolation between independently trained models is unstable (Fig. 4b). Aligning the larger model's latents to the smaller model's distribution before interpolation yields consistent gains across the mixing range. As shown in Fig. 4a, small injections from the source ($\lambda \in [0.05, 0.20]$) deliver the best improvements over the `Gemma-3-1B-it` baseline.

Cross-family (LLaMA-3.2-1B-instruct $\rightarrow$ Gemma-3-1B-it). Family-level transfer is more challenging: baseline parameter/latent mixing without alignment degrades performance. Table 5 shows that distributionally aligned latent merging recovers and surpasses these baselines, a modest interpolation weight ($\lambda = 0.1$) achieves the best overall scores. The evaluation for cross family evaluation is performed using *lm-eval* for simplicity and also due to some issues with llama model when using the previous evaluation code.

Takeaway. *Matching latent dimensionality* is insufficient for heterogeneous merges, *aligning latent distributions* is crucial. Once aligned, a single knob λ reliably controls how much capacity is injected from the source into the target.

5 Ablation Studies

To better understand the properties of our method, we conduct two targeted ablation studies. In this section we use *lm-eval* for evaluation unless stated.

Strategy	WinoGrande	ARC-C	HellaSwag
Base	56.83	42.78	49.07
OT only	51.13	34.25	48.50
OT + interp.	**57.75**	**43.34**	**50.10**

Table 5: Downstream accuracy on WinoGrande, ARC-Challenge, and HellaSwag for different alignment strategies with $\lambda = 0.1$.

Strategy	WinoGrande	ARC-C	MMLU
Base	56.83	42.78	40.76
MLP	56.84	**43.89**	41.02
Attention	56.67	40.23	39.80
Attention + MLP	**57.75**	43.34	**42.10**

Table 6: Ablation: Merging subsets of layers. MLP-only outperforms on ARC-C, combining MLP and Attention achieves the best results.

Model	Winogrande (5-shot)	ARC-Challenge (25-shot)	HellaSwag (10-shot)	MMLU (5-shot)
Gemma-3-1B-it (base)	56.83	42.78	49.07	40.76
LLaMA-3.2-1B-it (base)	61.56	41.11	61.62	46.55
Gemma-3-1B-it (VAE, $r = 1.6$)	56.67	42.83	47.31	39.98
LLaMA-3.2-1B-it (VAE, $r = 1.6$)	61.25	41.47	60.80	46.06
Gemma-3-1B-it (VAE, $r = 2$)	56.67	38.23	38.88	32.22
LLaMA-3.2-1B-it (VAE, $r = 2$)	59.43	37.12	55.99	39.73
Gemma-3-1B-it (VAE, $r = 4$)	46.49	28.24	25.66	25.02
LLaMA-3.2-1B-it (VAE, $r = 4$)	49.20	26.28	25.70	26.76

Table 7: Accuracy of VAE models (trained on `Gemma-3-4B-it`) when evaluated on `Gemma-3-1B-it` and `LLaMA-3.2-1B-it`. Performance remains stable for $r = 1.6$, but deteriorates as the compression factor increases.

5.1 Component Contributions in Latent Merging

We first analyze how different submodules contribute to the merged model's performance by merging MLP layers only, self-attention layers only, or both jointly. The results in Table 6 show that merging MLP layers alone provides modest gains, while merging attention layers alone degrades performance. Optimal results are achieved by merging both, indicating that **MLP and self-attention parameters encode complementary functional knowledge**, and that altering one without the other can disrupt learned co-adaptations.

5.2 VAE Generalization and the Compression Trade-off

Next, we assess the VAE's zero-shot generalization by training it on `Gemma-3-4B-it` and evaluating it on two unseen models: an in-family `Gemma-3-1B-it` and an out-of-family `LLaMA-3.2-1B-it`. Table 7 reveals a clear trade-off between compression and generalization. At a low compression ratio ($r = 1.6$), the VAE maintains strong performance on both unseen models. However, performance degrades substantially at higher ratios ($r = 2, 4$). This suggests that while the VAE learns transferable representations of weight structures, higher compression ratios lead to posterior collapse due to the fact most of the data sample are cluster aroung zero.

5.3 Linear Subspace vs. Non-Linear Manifold Learning

In this section we investigate the use of incremental PCA for weights encoding on gemma-3-1 b-it compare to VAE based en coding. Although Section 3.1 showed that LLM weight matrices exhibit low-rank structure, this does not imply that the space of functional parameters forms a linear subspace. To assess whether linear methods are sufficient, we compare our non-linear Transformer-VAE against PCA across compression ratios $r \in \{1.6, 2.0, 4.0\}$ (Table 8).

PCA collapses functional performance. Across all ratios, PCA-reconstructed models regress to near-random accuracy on MMLU ($\approx$25.5% at $r = 1.6$) and exhibit a global drop across benchmarks (e.g., ARC-C: 42.41% $\rightarrow$ 27.65%). Notably, performance is equally poor at $r = 1.6$ and $r = 4.0$, indicating that the failure is not due to insufficient latent capacity but to a structural mismatch: the set of valid pretrained weights does not reside in a linear subspace.

VAE preserves the functional manifold. In contrast, the LS-Merge VAE retains near-original accuracy at all compression levels. At $r = 1.6$, it recovers 96% of the base model's MMLU performance (39.89% vs. 41.44%) and even improves Winogrande (56.64% vs. 55.41%). Remarkably,

Table 8: Functional Reconstruction Fidelity vs. Compression Ratio. Zero-shot accuracy comparison on standard benchmarks (MMLU, HellaSwag, Winogrande, ARC-C) for Gemma-3-1B-it. We compare our non-linear Transformer-VAE (LS-Merge) against a linear PCA baseline at compression ratios $r \in \{1.6, 2, 4\}$. While the VAE maintains strong performance at $r = 1.6$ and $r = 2$, linear compression suffers significantly as the bottleneck tightens, validating the need for non-linear manifold learning.

Method	Ratio (r)	MMLU	HellaSwag	Winogrande	ARC-C
Gemma-3–1b-it)	1.0×	41.44 ± 0.00	49.05 ± 0.01	55.41 ± 0.03	42.41 ± 0.02
PCA (Linear)	1.6×	25.50 ± 0.37	25.56 ± 0.04	50.12 ± 0.01	27.65 ± 0.01
LS-Merge VAE	1.6×	**39.89** ± 0.01	**48.57** ± 0.25	**56.64** ± 0.15	**41.64** ± 0.01
PCA (Linear)	2.0×	24.12 ± 0.00	25.27 ± 0.12	46.27 ± 0.01	26.24 ± 0.32
LS-Merge VAE	2.0×	**39.80** ± 0.00	**49.29** ± 0.10	**54.14** ± 1.02	**42.32** ± 0.21
PCA (Linear)	4.0×	24.13 ± 0.15	24.79 ± 0.23	49.57 ± 0.01	25.89 ± 0.23
LS-Merge VAE	4.0×	**39.83** ± 0.00	**49.30** ± 0.21	**56.06** ± 0.15	**42.75** ± 0.20

VAE reconstructions remain stable at $r = 4.0$, whereas PCA has already collapsed at $r = 1.6$. This indicates that pretrained weights lie on a non-linear manifold that requires expressive encoders and decoders to model its curvature. Linear projections such as PCA cannot preserve the structure of the pretrained weight manifold and produce functionally invalid models even under mild compression. The VAE's non-linear latent geometry is therefore not a stylistic preference but a geometric necessity for faithful reconstruction, compression, and downstream operations such as interpolation and merging.

6 Discussion

Limitations Despite its strong performance, our approach has limitations. The training of the weight-encoding VAE is computationally non-trivial when for higher compression ratios and can be sensitive to hyperparameters, especially given the heavy-tailed nature of LLM weight distributions.

Future Work This work opens several avenues for future research. One direction is to explore more efficient or powerful generative models for weight encoding, such as extending latent-space merging to encompass more than two models via barycentric interpolation in the aligned latent space could unlock more complex model compositions.

7 Conclusion

In this work, we introduced LS-Merge, a novel framework that reimagines model merging by operating in a learned latent space of model parameters. By mapping weights to a continuous manifold and critically employing OT for principled alignment, our method successfully merges models with heterogeneous architectures, overcoming a fundamental limitation of prior weight-space techniques. Our comprehensive experiments demonstrate that this approach not only excels at standard expert fusion but also enables robust cross-scale and cross-family model merging for the first time. LS-Merge establishes a scalable and architecture-agnostic paradigm for model composition, paving the way for more flexible and efficient reuse of pre-trained models.

Reproducibility Statement

To ensure reliable and reproducible results, we have provided detailed experiment settings in the Appendix. We plan to open-source our implementation.

REFERENCES

Eirikur Agustsson, Alexander Sage, Radu Timofte, and Luc Van Gool. Optimal transport maps for distribution preserving operations on latent spaces of generative models. In *International Conference on Learning Representations*, 2019.

Takuya Akiba, Makoto Shing, Yujin Tang, Qi Sun, and David Ha. Evolutionary optimization of model merging recipes. *Nature Machine Intelligence*, 7(2):195–204, January 2025. ISSN 2522-5839. doi: 10.1038/s42256-024-00975-8. URL http://dx.doi.org/10.1038/s42256-024-00975-8.

Yoshua Bengio, Aaron C. Courville, and Pascal Vincent. Representation learning: A review and new perspectives. *IEEE Transactions on Pattern Analysis and Machine Intelligence*, 35:1798–1828, 2012.

Karl Cobbe, Vineet Kosaraju, Mohammad Bavarian, Mark Chen, Heewoo Jun, Lukasz Kaiser, Matthias Plappert, Jerry Tworek, Jacob Hilton, Reiichiro Nakano, Christopher Hesse, and John Schulman. Training verifiers to solve math word problems. *arXiv preprint arXiv:2110.14168*, 2021.

Wenxuan Ding, Shangbin Feng, Yuhan Liu, Zhaoxuan Tan, Vidhisha Balachandran, Tianxing He, and Yulia Tsvetkov. Knowledge crosswords: Geometric knowledge reasoning with large language models, 2024. URL https://arxiv.org/abs/2310.01290.

Carl Eckart and G. Marion Young. The approximation of one matrix by another of lower rank. *Psychometrika*, 1:211–218, 1936.

Shangbin Feng, Weijia Shi, Yike Wang, Wenxuan Ding, Vidhisha Balachandran, and Yulia Tsvetkov. Don't hallucinate, abstain: Identifying LLM knowledge gaps via multi-LLM collaboration. In *Proceedings of the 62nd Annual Meeting of the Association for Computational Linguistics (Volume 1: Long Papers)*, August 2024a.

Shangbin Feng, Zifeng Wang, Yike Wang, Sayna Ebrahimi, Hamid Palangi, Lesly Miculicich, Achin Kulshrestha, Nathalie Rauschmayr, Yejin Choi, Yulia Tsvetkov, Chen-Yu Lee, and Tomas Pfister. Model swarms: Collaborative search to adapt llm experts via swarm intelligence, 2024b. URL https://arxiv.org/abs/2410.11163.

Rémi Flamary, Nicolas Courty, Alexandre Gramfort, Mokhtar Z. Alaya, Aurélie Boisbunon, Stanislas Chambon, Laetitia Chapel, Adrien Corenflos, Kilian Fatras, Nemo Fournier, Léo Gautheron, Nathalie T.H. Gayraud, Hicham Janati, Alain Rakotomamonjy, Ievgen Redko, Antoine Rolet, Antony Schutz, Vivien Seguy, Danica J. Sutherland, Romain Tavenard, Alexander Tong, and Titouan Vayer. Pot: Python optimal transport. *Journal of Machine Learning Research*, 22(78):1–8, 2021. URL http://jmlr.org/papers/v22/20-451.html.

Rémi Flamary, Cédric Vincent-Cuaz, Nicolas Courty, Alexandre Gramfort, Oleksii Kachaiev, Huy Quang Tran, Laurène David, Clément Bonet, Nathan Cassereau, Théo Gnassounou, Eloi Tanguy, Julie Delon, Antoine Collas, Sonia Mazelet, Laetitia Chapel, Tanguy Kerdoncuff, Xizheng Yu, Matthew Feickert, Paul Krzakala, Tianlin Liu, and Eduardo Fernandes Montesuma. Pot python optimal transport (version 0.9.5), 2024. URL https://github.com/PythonOT/POT.

Leo Gao, Jonathan Tow, Baber Abbasi, Stella Biderman, Sid Black, Anthony DiPofi, Charles Foster, Laurence Golding, Jeffrey Hsu, Alain Le Noac'h, Haonan Li, Kyle McDonell, Niklas Muennighoff, Chris Ociepa, Jason Phang, Laria Reynolds, Hailey Schoelkopf, Aviya Skowron, Lintang Sutawika, Eric Tang, Anish Thite, Ben Wang, Kevin Wang, and Andy Zou. The language model evaluation harness, 07 2024. URL https://zenodo.org/records/12608602.

Aaron Grattafiori, Abhimanyu Dubey, Abhinav Jauhri, Abhinav Pandey, Abhishek Kadian, Ahmad Al-Dahle, Aiesha Letman, Akhil Mathur, Alan Schelten, Alex Vaughan, Amy Yang, Angela Fan, Anirudh Goyal, Anthony Hartshorn, Aobo Yang, Archi Mitra, Archie Sravankumar, Artem Korenev, Arthur Hinsvark, Arun Rao, Aston Zhang, Aurelien Rodriguez, Austen Gregerson, Ava Spataru, Baptiste Roziere, Bethany Biron, Binh Tang, Bobbie Chern, Charlotte Caucheteux, Chaya Nayak, Chloe Bi, Chris Marra, Chris McConnell, Christian Keller, Christophe Touret, Chunyang

Wu, Corinne Wong, Cristian Canton Ferrer, Cyrus Nikolaidis, Damien Allonsius, Daniel Song, Danielle Pintz, Danny Livshits, Danny Wyatt, David Esiobu, Dhruv Choudhary, Dhruv Mahajan, Diego Garcia-Olano, Diego Perino, Dieuwke Hupkes, Egor Lakomkin, Ehab AlBadawy, Elina Lobanova, Emily Dinan, Eric Michael Smith, Filip Radenovic, Francisco Guzmán, Frank Zhang, Gabriel Synnaeve, Gabrielle Lee, Georgia Lewis Anderson, Govind Thattai, Graeme Nail, Gregoire Mialon, Guan Pang, Guillem Cucurell, Hailey Nguyen, Hannah Korevaar, Hu Xu, Hugo Touvron, Iliyan Zarov, Imanol Arrieta Ibarra, Isabel Kloumann, Ishan Misra, Ivan Evtimov, Jack Zhang, Jade Copet, Jaewon Lee, Jan Geffert, Jana Vranes, Jason Park, Jay Mahadeokar, Jeet Shah, Jelmer van der Linde, Jennifer Billock, Jenny Hong, Jenya Lee, Jeremy Fu, Jianfeng Chi, Jianyu Huang, Jiawen Liu, Jie Wang, Jiecao Yu, Joanna Bitton, Joe Spisak, Jongsoo Park, Joseph Rocca, Joshua Johnstun, Joshua Saxe, Junteng Jia, Kalyan Vasuden Alwala, Karthik Prasad, Kartikeya Upasani, Kate Plawiak, Ke Li, Kenneth Heafield, Kevin Stone, Khalid El-Arini, Krithika Iyer, Kshitiz Malik, Kuenley Chiu, Kunal Bhalla, Kushal Lakhotia, Lauren Rantala-Yeary, Laurens van der Maaten, Lawrence Chen, Liang Tan, Liz Jenkins, Louis Martin, Lovish Madaan, Lubo Malo, Lukas Blecher, Lukas Landzaat, Luke de Oliveira, Madeline Muzzi, Mahesh Pasupuleti, Mannat Singh, Manohar Paluri, Marcin Kardas, Maria Tsimpoukelli, Mathew Oldham, Mathieu Rita, Maya Pavlova, Melanie Kambadur, Mike Lewis, Min Si, Mitesh Kumar Singh, Mona Hassan, Naman Goyal, Narjes Torabi, Nikolay Bashlykov, Nikolay Bogoychev, Niladri Chatterji, Ning Zhang, Olivier Duchenne, Onur Çelebi, Patrick Alrassy, Pengchuan Zhang, Pengwei Li, Petar Vasic, Peter Weng, Prajjwal Bhargava, Pratik Dubal, Praveen Krishnan, Punit Singh Koura, Puxin Xu, Qing He, Qingxiao Dong, Ragavan Srinivasan, Raj Ganapathy, Ramon Calderer, Ricardo Silveira Cabral, Robert Stojnic, Roberta Raileanu, Rohan Maheswari, Rohit Girdhar, Rohit Patel, Romain Sauvestre, Ronnie Polidoro, Roshan Sumbaly, Ross Taylor, Ruan Silva, Rui Hou, Rui Wang, Saghar Hosseini, Sahana Chennabasappa, Sanjay Singh, Sean Bell, Seohyun Sonia Kim, Sergey Edunov, Shaoliang Nie, Sharan Narang, Sharath Raparthy, Sheng Shen, Shengye Wan, Shruti Bhosale, Shun Zhang, Simon Vandenhende, Soumya Batra, Spencer Whitman, Sten Sootla, Stephane Collot, Suchin Gururangan, Sydney Borodinsky, Tamar Herman, Tara Fowler, Tarek Sheasha, Thomas Georgiou, Thomas Scialom, Tobias Speckbacher, Todor Mihaylov, Tong Xiao, Ujjwal Karn, Vedanuj Goswami, Vibhor Gupta, Vignesh Ramanathan, Viktor Kerkez, Vincent Gonguet, Virginie Do, Vish Vogeti, Vítor Albiero, Vladan Petrovic, Weiwei Chu, Wenhan Xiong, Wenyin Fu, Whitney Meers, Xavier Martinet, Xiaodong Wang, Xiaofang Wang, Xiaoqing Ellen Tan, Xide Xia, Xinfeng Xie, Xuchao Jia, Xuewei Wang, Yaelle Goldschlag, Yashesh Gaur, Yasmine Babaei, Yi Wen, Yiwen Song, Yuchen Zhang, Yue Li, Yuning Mao, Zacharie Delpierre Coudert, Zheng Yan, Zhengxing Chen, Zoe Papakipos, Aaditya Singh, Aayushi Srivastava, Abha Jain, Adam Kelsey, Adam Shajnfeld, Adithya Gangidi, Adolfo Victoria, Ahuva Goldstand, Ajay Menon, Ajay Sharma, Alex Boesenberg, Alexei Baevski, Allie Feinstein, Amanda Kallet, Amit Sangani, Amos Teo, Anam Yunus, Andrei Lupu, Andres Alvarado, Andrew Caples, Andrew Gu, Andrew Ho, Andrew Poulton, Andrew Ryan, Ankit Ramchandani, Annie Dong, Annie Franco, Anuj Goyal, Aparajita Saraf, Arkabandhu Chowdhury, Ashley Gabriel, Ashwin Bharambe, Assaf Eisenman, Azadeh Yazdan, Beau James, Ben Maurer, Benjamin Leonhardi, Bernie Huang, Beth Loyd, Beto De Paola, Bhargavi Paranjape, Bing Liu, Bo Wu, Boyu Ni, Braden Hancock, Bram Wasti, Brandon Spence, Brani Stojkovic, Brian Gamido, Britt Montalvo, Carl Parker, Carly Burton, Catalina Mejia, Ce Liu, Changhan Wang, Changkyu Kim, Chao Zhou, Chester Hu, Ching-Hsiang Chu, Chris Cai, Chris Tindal, Christoph Feichtenhofer, Cynthia Gao, Damon Civin, Dana Beaty, Daniel Kreymer, Daniel Li, David Adkins, David Xu, Davide Testuggine, Delia David, Devi Parikh, Diana Liskovich, Didem Foss, Dingkang Wang, Duc Le, Dustin Holland, Edward Dowling, Eissa Jamil, Elaine Montgomery, Eleonora Presani, Emily Hahn, Emily Wood, Eric-Tuan Le, Erik Brinkman, Esteban Arcaute, Evan Dunbar, Evan Smothers, Fei Sun, Felix Kreuk, Feng Tian, Filippos Kokkinos, Firat Ozgenel, Francesco Caggioni, Frank Kanayet, Frank Seide, Gabriela Medina Florez, Gabriella Schwarz, Gada Badeer, Georgia Swee, Gil Halpern, Grant Herman, Grigory Sizov, Guangyi, Zhang, Guna Lakshminarayanan, Hakan Inan, Hamid Shojanazeri, Han Zou, Hannah Wang, Hanwen Zha, Haroun Habeeb, Harrison Rudolph, Helen Suk, Henry Aspegren, Hunter Goldman, Hongyuan Zhan, Ibrahim Damlaj, Igor Molybog, Igor Tufanov, Ilias Leontiadis, Irina-Elena Veliche, Itai Gat, Jake Weissman, James Geboski, James Kohli, Janice Lam, Japhet Asher, Jean-Baptiste Gaya, Jeff Marcus, Jeff Tang, Jennifer Chan, Jenny Zhen, Jeremy Reizenstein, Jeremy Teboul, Jessica Zhong, Jian Jin, Jingyi Yang, Joe Cummings, Jon Carvill, Jon Shepard, Jonathan McPhie, Jonathan Torres, Josh Ginsburg, Junjie Wang, Kai Wu, Kam Hou U, Karan Saxena, Kartikay Khandelwal, Katayoun Zand, Kathy Matosich, Kaushik Veeraraghavan, Kelly Michelena, Keqian Li, Kiran Jagadeesh, Kun Huang, Kunal Chawla, Kyle Huang, Lailin Chen, Lakshya Garg, Lavender A,

Leandro Silva, Lee Bell, Lei Zhang, Liangpeng Guo, Licheng Yu, Liron Moshkovich, Luca Wehrstedt, Madian Khabsa, Manav Avalani, Manish Bhatt, Martynas Mankus, Matan Hasson, Matthew Lennie, Matthias Reso, Maxim Groshev, Maxim Naumov, Maya Lathi, Meghan Keneally, Miao Liu, Michael L. Seltzer, Michal Valko, Michelle Restrepo, Mihir Patel, Mik Vyatskov, Mikayel Samvelyan, Mike Clark, Mike Macey, Mike Wang, Miquel Jubert Hermoso, Mo Metanat, Mohammad Rastegari, Munish Bansal, Nandhini Santhanam, Natascha Parks, Natasha White, Navyata Bawa, Nayan Singhal, Nick Egebo, Nicolas Usunier, Nikhil Mehta, Nikolay Pavlovich Laptev, Ning Dong, Norman Cheng, Oleg Chernoguz, Olivia Hart, Omkar Salpekar, Ozlem Kalinli, Parkin Kent, Parth Parekh, Paul Saab, Pavan Balaji, Pedro Rittner, Philip Bontrager, Pierre Roux, Piotr Dollar, Polina Zvyagina, Prashant Ratanchandani, Pritish Yuvraj, Qian Liang, Rachad Alao, Rachel Rodriguez, Rafi Ayub, Raghotham Murthy, Raghu Nayani, Rahul Mitra, Rangaprabhu Parthasarathy, Raymond Li, Rebekkah Hogan, Robin Battey, Rocky Wang, Russ Howes, Ruty Rinott, Sachin Mehta, Sachin Siby, Sai Jayesh Bondu, Samyak Datta, Sara Chugh, Sara Hunt, Sargun Dhillon, Sasha Sidorov, Satadru Pan, Saurabh Mahajan, Saurabh Verma, Seiji Yamamoto, Sharadh Ramaswamy, Shaun Lindsay, Shaun Lindsay, Sheng Feng, Shenghao Lin, Shengxin Cindy Zha, Shishir Patil, Shiva Shankar, Shuqiang Zhang, Shuqiang Zhang, Sinong Wang, Sneha Agarwal, Soji Sajuyigbe, Soumith Chintala, Stephanie Max, Stephen Chen, Steve Kehoe, Steve Satterfield, Sudarshan Govindaprasad, Sumit Gupta, Summer Deng, Sungmin Cho, Sunny Virk, Suraj Subramanian, Sy Choudhury, Sydney Goldman, Tal Remez, Tamar Glaser, Tamara Best, Thilo Koehler, Thomas Robinson, Tianhe Li, Tianjun Zhang, Tim Matthews, Timothy Chou, Tzook Shaked, Varun Vontimitta, Victoria Ajayi, Victoria Montanez, Vijai Mohan, Vinay Satish Kumar, Vishal Mangla, Vlad Ionescu, Vlad Poenaru, Vlad Tiberiu Mihailescu, Vladimir Ivanov, Wei Li, Wenchen Wang, Wenwen Jiang, Wes Bouaziz, Will Constable, Xiaocheng Tang, Xiaojian Wu, Xiaolan Wang, Xilun Wu, Xinbo Gao, Yaniv Kleinman, Yanjun Chen, Ye Hu, Ye Jia, Ye Qi, Yenda Li, Yilin Zhang, Ying Zhang, Yossi Adi, Youngjin Nam, Yu, Wang, Yu Zhao, Yuchen Hao, Yundi Qian, Yunlu Li, Yuzi He, Zach Rait, Zachary DeVito, Zef Rosnbrick, Zhaoduo Wen, Zhenyu Yang, Zhiwei Zhao, and Zhiyu Ma. The llama 3 herd of models, 2024.

Suchin Gururangan, Margaret Li, Mike Lewis, Weijia Shi, Tim Althoff, Noah A. Smith, and Luke Zettlemoyer. Scaling expert language models with unsupervised domain discovery. *arXiv preprint arXiv:2303.14177*, 2023.

Dan Hendrycks, Collin Burns, Steven Basart, Andy Zou, Mantas Mazeika, Dawn Song, and Jacob Steinhardt. Measuring massive multitask language understanding. *Proceedings of the International Conference on Learning Representations (ICLR)*, 2021.

Chengsong Huang, Qian Liu, Bill Yuchen Lin, Tianyu Pang, Chao Du, and Min Lin. Lorahub: Efficient cross-task generalization via dynamic lora composition, 2023.

Gabriel Ilharco, Marco Tulio Ribeiro, Mitchell Wortsman, Ludwig Schmidt, Hannaneh Hajishirzi, and Ali Farhadi. Editing models with task arithmetic. In *The Eleventh International Conference on Learning Representations*, 2023. URL https://openreview.net/forum?id=6t0Kwf8-jrj.

Dong-Hwan Jang, Sangdoo Yun, and Dongyoon Han. Model stock: All we need is just a few fine-tuned models. In *Proceedings of the European Conference on Computer Vision*, 2024.

Diederik P. Kingma and Max Welling. Auto-encoding variational bayes. *CoRR*, abs/1312.6114, 2013. URL https://api.semanticscholar.org/CorpusID:216078090.

Ivan Kobyzev, Simon J.D. Prince, and Marcus A. Brubaker. Normalizing flows: An introduction and review of current methods. *IEEE Transactions on Pattern Analysis and Machine Intelligence*, 43 (11):3964–3979, 2021. doi: 10.1109/TPAMI.2020.2992934.

Subhaneil Lahiri, Peiran Gao, and Surya Ganguli. Random projections of random manifolds, 2016. URL https://arxiv.org/abs/1607.04331.

Stephanie Lin, Jacob Hilton, and Owain Evans. Truthfulqa: Measuring how models mimic human falsehoods, 2022. URL https://arxiv.org/abs/2109.07958.

Costas Mavromatis, Petros Karypis, and George Karypis. Pack of llms: Model fusion at test-time via perplexity optimization. *ArXiv*, abs/2404.11531, 2024. URL https://api.semanticscholar.org/CorpusID:269188153.

Amin Heyrani Nobari, Kaveh Alimohammadi, Ali ArjomandBigdeli, Akash Srivastava, Faez Ahmed, and Navid Azizan. Activation-informed merging of large language models, 2025. URL https://arxiv.org/abs/2502.02421.

Filippo Santambrogio. *Optimal Transport for Applied Mathematicians: Calculus of Variations, PDEs, and Modeling*, volume 87 of *Progress in Nonlinear Differential Equations and Their Applications*. Birkhäuser, 2015.

Konstantin Sch"urholt, Michael W. Mahoney, and Damian Borth. Towards scalable and versatile weight space learning. In *Proceedings of the 41st International Conference on Machine Learning (ICML)*, 2024.

Chongjie Si, Jingjing Jiang, and Wei Shen. Unveiling the mystery of weight in large foundation models: Gaussian distribution never fades, 2025.

Bedionita Soro, Bruno Andreis, Hayeon Lee, Wonyong Jeong, Song Chong, Frank Hutter, and Sung Ju Hwang. Diffusion-based neural network weights generation. In *The Thirteenth International Conference on Learning Representations*, 2025.

Gemma Team, Aishwarya Kamath, Johan Ferret, Shreya Pathak, Nino Vieillard, Ramona Merhej, Sarah Perrin, Tatiana Matejovicova, Alexandre Ramé, Morgane Rivière, Louis Rouillard, Thomas Mesnard, Geoffrey Cideron, Jean bastien Grill, Sabela Ramos, Edouard Yvinec, Michelle Casbon, Etienne Pot, Ivo Penchev, Gaël Liu, Francesco Visin, Kathleen Kenealy, Lucas Beyer, Xiaohai Zhai, Anton Tsitsulin, Robert Busa-Fekete, Alex Feng, Noveen Sachdeva, Benjamin Coleman, Yi Gao, Basil Mustafa, Iain Barr, Emilio Parisotto, David Tian, Matan Eyal, Colin Cherry, Jan-Thorsten Peter, Danila Sinopalnikov, Surya Bhupatiraju, Rishabh Agarwal, Mehran Kazemi, Dan Malkin, Ravin Kumar, David Vilar, Idan Brusilovsky, Jiaming Luo, Andreas Steiner, Abe Friesen, Abhanshu Sharma, Abheesht Sharma, Adi Mayrav Gilady, Adrian Goedeckemeyer, Alaa Saade, Alex Feng, Alexander Kolesnikov, Alexei Bendebury, Alvin Abdagic, Amit Vadi, András György, André Susano Pinto, Anil Das, Ankur Bapna, Antoine Miech, Antoine Yang, Antonia Paterson, Ashish Shenoy, Ayan Chakrabarti, Bilal Piot, Bo Wu, Bobak Shahriari, Bryce Petrini, Charlie Chen, Charline Le Lan, Christopher A. Choquette-Choo, CJ Carey, Cormac Brick, Daniel Deutsch, Danielle Eisenbud, Dee Cattle, Derek Cheng, Dimitris Paparas, Divyashree Shivakumar Sreepathihalli, Doug Reid, Dustin Tran, Dustin Zelle, Eric Noland, Erwin Huizenga, Eugene Kharitonov, Frederick Liu, Gagik Amirkhanyan, Glenn Cameron, Hadi Hashemi, Hanna Klimczak-Plucińska, Harman Singh, Harsh Mehta, Harshal Tushar Lehri, Hussein Hazimeh, Ian Ballantyne, Idan Szpektor, Ivan Nardini, Jean Pouget-Abadie, Jetha Chan, Joe Stanton, John Wieting, Jonathan Lai, Jordi Orbay, Joseph Fernandez, Josh Newlan, Ju yeong Ji, Jyotinder Singh, Kat Black, Kathy Yu, Kevin Hui, Kiran Vodrahalli, Klaus Greff, Linhai Qiu, Marcella Valentine, Marina Coelho, Marvin Ritter, Matt Hoffman, Matthew Watson, Mayank Chaturvedi, Michael Moynihan, Min Ma, Nabila Babar, Natasha Noy, Nathan Byrd, Nick Roy, Nikola Momchev, Nilay Chauhan, Noveen Sachdeva, Oskar Bunyan, Pankil Botarda, Paul Caron, Paul Kishan Rubenstein, Phil Culliton, Philipp Schmid, Pier Giuseppe Sessa, Pingmei Xu, Piotr Stanczyk, Pouya Tafti, Rakesh Shivanna, Renjie Wu, Renke Pan, Reza Rokni, Rob Willoughby, Rohith Vallu, Ryan Mullins, Sammy Jerome, Sara Smoot, Sertan Girgin, Shariq Iqbal, Shashir Reddy, Shruti Sheth, Siim Põder, Sijal Bhatnagar, Sindhu Raghuram Panyam, Sivan Eiger, Susan Zhang, Tianqi Liu, Trevor Yacovone, Tyler Liechty, Uday Kalra, Utku Evci, Vedant Misra, Vincent Roseberry, Vlad Feinberg, Vlad Kolesnikov, Woohyun Han, Woosuk Kwon, Xi Chen, Yinlam Chow, Yuvein Zhu, Zichuan Wei, Zoltan Egyed, Victor Cotruta, Minh Giang, Phoebe Kirk, Anand Rao, Kat Black, Nabila Babar, Jessica Lo, Erica Moreira, Luiz Gustavo Martins, Omar Sanseviero, Lucas Gonzalez, Zach Gleicher, Tris Warkentin, Vahab Mirrokni, Evan Senter, Eli Collins, Joelle Barral, Zoubin Ghahramani, Raia Hadsell, Yossi Matias, D. Sculley, Slav Petrov, Noah Fiedel, Noam Shazeer, Oriol Vinyals, Jeff Dean, Demis Hassabis, Koray Kavukcuoglu, Clement Farabet, Elena Buchatskaya, Jean-Baptiste Alayrac, Rohan Anil, Dmitry, Lepikhin, Sebastian Borgeaud, Olivier Bachem, Armand Joulin, Alek Andreev, Cassidy Hardin, Robert Dadashi, and Léonard Hussenot. Gemma 3 technical report, 2025.

Ashish Vaswani, Noam Shazeer, Niki Parmar, Jakob Uszkoreit, Llion Jones, Aidan N Gomez, Ł ukasz Kaiser, and Illia Polosukhin. Attention is all you need. In I. Guyon, U. Von Luxburg, S. Bengio, H. Wallach, R. Fergus, S. Vishwanathan, and R. Garnett (eds.), *Advances in Neural Information Processing Systems*, volume 30. Curran Associates, Inc., 2017.

Cédric Villani. *Optimal Transport: Old and New*, volume 338 of *Grundlehren der mathematischen Wissenschaften*. Springer, 2009.

Heng Wang, Shangbin Feng, Tianxing He, Zhaoxuan Tan, Xiaochuang Han, and Yulia Tsvetkov. Can language models solve graph problems in natural language?, 2024a. URL https://arxiv.org/abs/2305.10037.

Kai Wang, Dongwen Tang, Wangbo Zhao, Konstantin Schürholt, Zhangyang Wang, and Yang You. Recurrent diffusion for large-scale parameter generation, 2025.

Yubo Wang, Xueguang Ma, Ge Zhang, Yuansheng Ni, Abhranil Chandra, Shiguang Guo, Weiming Ren, Aaran Arulraj, Xuan He, Ziyan Jiang, et al. Mmlu-pro: A more robust and challenging multi-task language understanding benchmark. *arXiv preprint arXiv:2406.01574*, 2024b.

Mitchell Wortsman, Gabriel Ilharco, Samir Ya Gadre, Rebecca Roelofs, Raphael Gontijo-Lopes, Ari S Morcos, Hongseok Namkoong, Ali Farhadi, Yair Carmon, Simon Kornblith, and Ludwig Schmidt. Model soups: averaging weights of multiple fine-tuned models improves accuracy without increasing inference time. In *Proceedings of the 39th International Conference on Machine Learning*, pp. 23965–23998, 2022.

Prateek Yadav, Derek Tam, Leshem Choshen, Colin Raffel, and Mohit Bansal. TIES-merging: Resolving interference when merging models. In *Thirty-seventh Conference on Neural Information Processing Systems*, 2023. URL https://openreview.net/forum?id=xtaX3WyCj1.

Enneng Yang, Li Shen, Guibing Guo, Xingwei Wang, Xiaochun Cao, Jie Zhang, and Dacheng Tao. Model merging in llms, mllms, and beyond: Methods, theories, applications and opportunities, 2024.

Le Yu, Bowen Yu, Haiyang Yu, Fei Huang, and Yongbin Li. Language models are super mario: absorbing abilities from homologous models as a free lunch. In *Proceedings of the 41st International Conference on Machine Learning*, ICML'24. JMLR.org, 2024a.

Le Yu, Bowen Yu, Haiyang Yu, Fei Huang, and Yongbin Li. Language models are super mario: Absorbing abilities from homologous models as a free lunch. In *International Conference on Machine Learning*, 2024b.

Rowan Zellers, Ari Holtzman, Yonatan Bisk, Ali Farhadi, and Yejin Choi. Hellaswag: Can a machine really finish your sentence?, 2019. URL https://arxiv.org/abs/1905.07830.

A Appendix

Impact Statement

We introduce a VAE-based latent-space merging technique for pretrained LLMs that encodes weights into compact codes, blends them, and decoding new high-performance parameters. This enables fast, compute-efficient model customization and smooth interpolation across architectures. However, blending latent codes can unintentionally merge biases or toxic behaviors, obscure the origin of capabilities, and be misused to graft malicious functionality. We advocate for rigorous bias / toxicity audits, transparent provenance tracking, and clear reporting guidelines to ensure responsible deployment.

A Extended Distribution Analysis

Section 3.1 characterized layerwise weight statistics to inform encoding and merging. Here we extend that analysis with (i) complete per-layer distribution plots, including all *MLP* layers for Gemma-3-1B-IT, Gemma-3-4B-IT, and LLaMA-3.2-3B-Instruct, and (ii) cumulative variance–explained curves from PCA on those MLP layers.

A.1 Data and procedure

Models. Gemma-3-1B-IT, Gemma-3-4B-IT, LLaMA-3.2-3B-Instruct, plus the main-paper models.

Layer selection. For each transformer block, we analyze *self-attention* (Q/K/V/O projections) and *MLP* (up/gate/down) weight matrices independently.

Preprocessing. Unless noted, statistics are computed on raw matrix entries. For PCA, matrices are mean-centered and the spectrum is computed over flattened rows; we report cumulative variance explained. We use *excess kurtosis* (Fisher convention) so a Gaussian has $\kappa_{\text{ex}}=0$:

$$\kappa_{\text{ex}} = \frac{\mathbb{E}[(W-\mu)^4]}{\sigma^4} - 3.$$

Means and variances are standard sample estimates; skewness uses the unbiased estimator.

Aggregation. We report per-layer curves and layer-type aggregates (self-attention vs. MLP). Family summaries first average across layers within a model, then across models in the same family.

A.2 Complete plots

Figure 5 shows layerwise distribution plots (self-attention and MLP). Figure 6 reports cumulative PCA variance for all MLP layers (attention spectra are in the main text).

A.3 Findings and implications

Self-attention layers exhibit heavier tails in Gemma. In self-attention projections (Fig. 7a, Table 9), Gemma-3-1B-IT and Gemma-3-4B-IT show pronounced positive excess kurtosis with depth-localized peaks, indicating heavy tails and more extreme outliers. LLaMA models track closely across scales, suggesting family-level statistical stability.

MLP layers are more stable and closer to Gaussian. Across models (Fig. 7b, Table 9), MLP projections are near-Gaussian with excess kurtosis typically in $[0, 2]$ and fewer depth-dependent spikes. Their PCA spectra (Fig. 6) decay faster than attention, indicating lower intrinsic dimensionality.

Design implications for encoding and merging.

- *Allocate capacity to attention.* Heavy tails in attention (notably in Gemma) warrant encoders with higher capacity or robust priors; Gaussian assumptions under-represent extremes.
- *MLP is the easy regime.* More Gaussian, stable MLP statistics admit accurate compression with standard VAE settings and fewer latent pathologies.
- *Family consistency aids calibration.* The alignment of LLaMA statistics across scales simplifies cross-scale latent calibration and reduces merging friction.

Summary. Attention weights (especially in Gemma) are the dominant source of heavy-tail behavior; MLP weights are comparatively benign. Tail-aware encoding and depthwise calibration are most critical for attention, while default settings suffice for MLP.

B Variational Encoder Architecture and Training Details

Table 10 lists the configuration of our transformer VAE. The encoder applies a twofold down-projection of the token (*compression ratio* $r=2$), which is the smallest bottleneck we found that preserves reconstruction while generalizing to unseen checkpoints. The decoder mirrors the encoder to restore the original dimension. For heterogeneous merges, we set the latent size d_z by the source to target layer mapping ratio and keep all other hyperparameters fixed, ensuring comparable latent scales across architectures.

Objective. We optimize the ELBO (reconstruction + KL to $\mathcal{N}(0, I)$) with a constant learning rate 1×10^{-5} for 10,000 epochs.

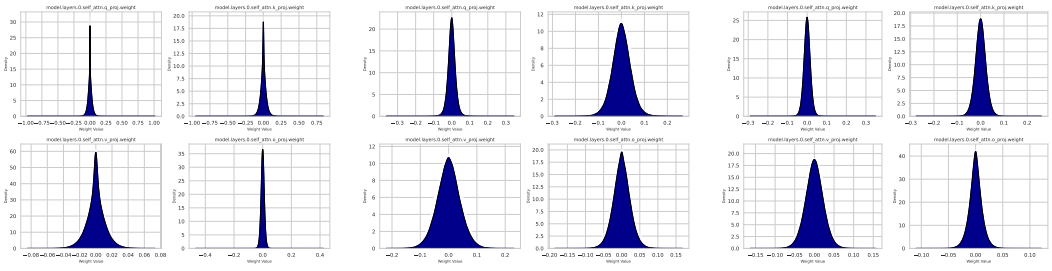

(a) llama3-2-3b-it-self_attn-layer0 (b) gemma-3-1b-it-self_attn-layer0 (c) gemma-3-4b-it-self_attn-layer0

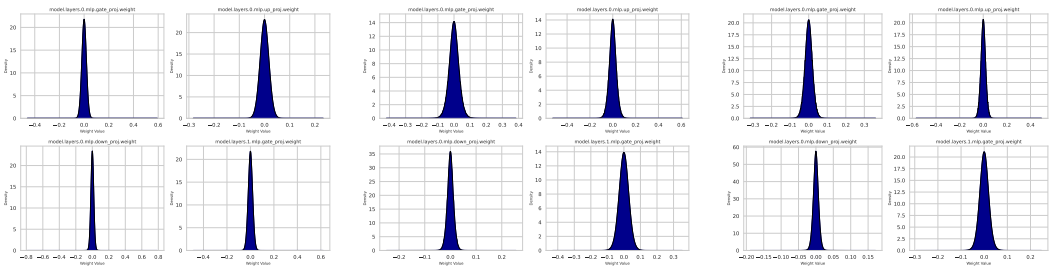

(d) llama3-2-3b-it-mlp-layer0-1 (e) gemma-3-1b-it-mlp-layer0-1 (f) gemma-3-4b-it-mlp-layer0-1

Figure 5: Distribution plot of the self-attention and the mlp modules in llama3-1-8b-instruct, gemma-3-1b-it, and gemma-3-4b-it for attention layer 0.

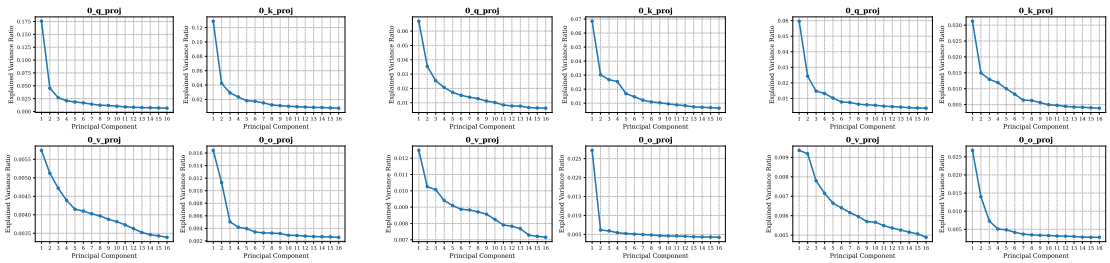

(a) Llama3-2-3b-it-self_attn-layer0 (b) Gemma-3-1b-it-self_attn-layer0 (c) Gemma-3-4b-it-self_attn-layer0

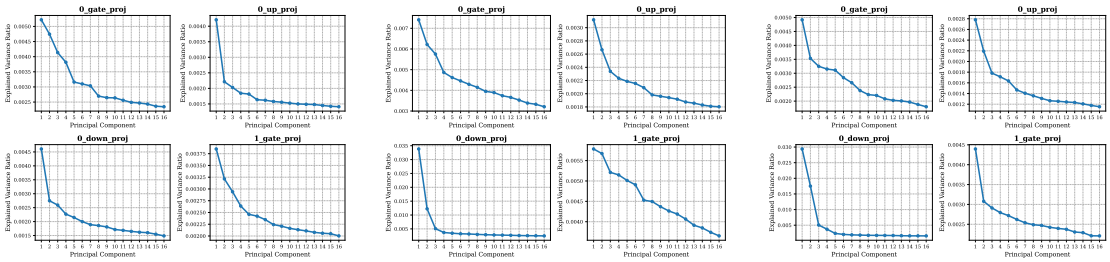

(d) Llama3-2-3b-it-mlp-layer0-1 (e) Gemma-3-1b-it-mlp-layer0-1 (f) Gemma-3-4b-it-mlp-layer0-1

Figure 6: Plots of the PCA **explained-variance ratio** for individual weight matrices in the first self-attention block (top row of each subpanel set) of three LLM checkpoints—Llama-3-2-3b-it, Gemma-3-1b-it, and Gemma-3-4b-it. For each model, we show the four projection matrices of self-attention (*q, k, v, o*). The sharp drop after the leading principal components highlights a pronounced low-rank structure that is consistent across architectures and model sizes.

Training setup. Single NVIDIA A6000, bfloat16 for forward and backward, the remaining settings (optimizer, batch size, weight decay, clip-norm) are in Table 10. Seeds are fixed for data order and initialization.

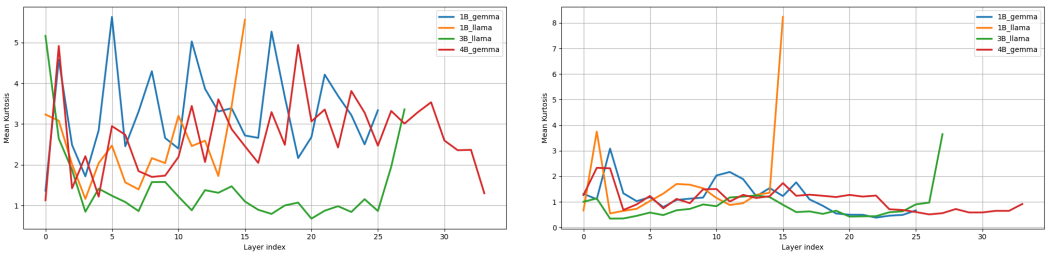

(a) Mean kurtosis per layer (Self-attention layers).

(b) Mean kurtosis per layer (MLP layers).

Figure 7: Comparison of mean kurtosis across layers in self-attention and MLP components for Gemma and LLaMA models.

layers	llama3-2-3b-it			gemma-3-1b-it			gemma-3-4b-it		
	var.	skew	kurt.	var.	skew	kurt.	var.	skew	kurt.
self_attn	0.0017	0.0192	8.4032	0.0031	0.0500	15.0505	0.0015	0.0501	15.2010
	0.0013	0.0191	7.3438	0.0030	0.0450	9.8347	0.0015	0.0267	7.3832
	0.0012	0.0178	6.2172	0.0030	0.0389	9.0363	0.0014	0.0255	7.2277
	0.0011	0.0104	5.4477	0.0030	0.0288	8.6496	0.0014	0.0172	6.0731
avg (self_attn)	0.0005	-0.0002	1.4342	0.0012	-0.0009	3.2858	0.0005	0.0009	2.6900
min (self_attn)	0.0001	-0.0131	0.3027	0.0002	-0.0418	0.1589	0.0001	-0.0305	0.2412
mlp	0.0005	0.0093	5.4740	0.0010	0.0167	8.7665	0.0004	0.0266	6.3297
	0.0005	0.0080	4.1465	0.0010	0.0090	3.1514	0.0004	0.0155	5.9670
	0.0004	0.0075	2.6694	0.0010	0.0077	3.0577	0.0004	0.0130	2.7454
	0.0004	0.0074	2.4364	0.0010	0.0071	3.0113	0.0004	0.0094	2.4371
avg (mlp)	0.0003	0.0003	0.8435	0.0006	0	1.1739	0.0003	0.0006	1.0807
min (mlp)	0.0003	-0.0139	0.0892	-0.0001	-0.0184	0.1552	0	-0.0076	0.1559

Table 9: Statistical moments of the self-attention and MLP layers across three models.

Field	Value	Notes
`length`	10,240	Sequence length processed
`n_layers`	6	Transformer depth
`chunk_size`	640	Per-token chunk width
`embed_dim`	768	Matches global `embed_dim`
`latent_dim`	640	Size of latent vector per chunk
`n_heads`	4	Attention heads
`rope_base`	20,000	RoPE base frequency
`conv`	`false`	No convolutional patching
`flatten`	`true`	Flatten to original shape.

Table 10: Transformer block settings shared by the encoder and decoder.

Ablation summary. Bottlenecks weaker than $r{=}2$ overfit and degrade out-of-distribution reconstruction, stronger bottlenecks raise reconstruction error and harm downstream merging. Choosing d_z via the mapping ratio stabilizes cross-architecture alignment without retuning.

B.1 Analysis Weights Encoding Evolution

Pretrained weight matrices exhibit substantial variation in tail behavior (high to near-zero excess kurtosis; cf. Section 3.1). We study how this variability interacts with the compression ratio r in the VAE and how it impacts generalization to unseen checkpoints.

Convergence vs. compression. Figure 8 shows a clear monotone effect: optimization slows as the bottleneck tightens. With $r{=}2$ (twofold down-projection), storage is halved and the reconstruction loss increases by only $\approx 6\%$; at $r{=}4$, the penalty rises to $\approx 10\%$. These curves set a practical operating point: $r{\approx}2$ balances footprint and fidelity with minimal training overhead.

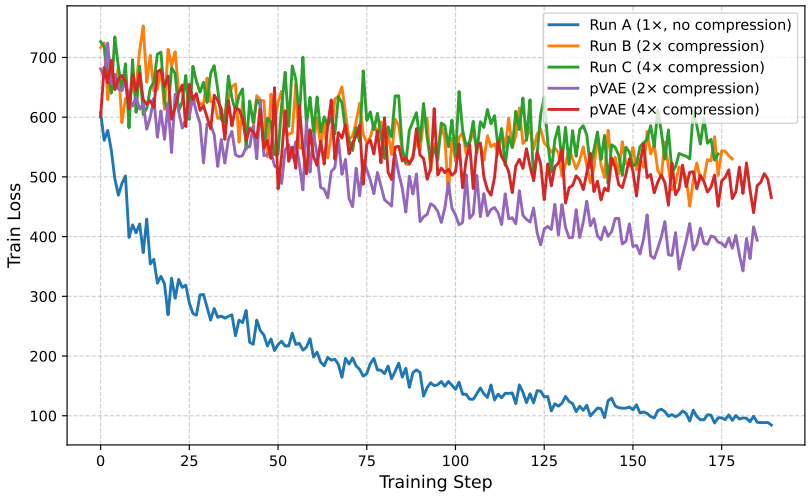

Figure 8: Mean reconstruction error curves (smoothed with a 5-step moving average) for pVAE (VAE initialized from an existing pretrained VAE with reduction factor 1) and VAE (random initialized VAE). r denotes the compression ratio.

Sensitivity to distribution shape. Layers with heavier tails (high excess kurtosis) are more sensitive to increasing r, exhibiting larger loss gaps at fixed training budget, near-Gaussian layers degrade more gently. In our models, attention projections in GEMMA fall into the former regime, whereas MLP projections across families align with the latter (App. A).

Training schedule. Two-Stage Training. To improve stability under tight bottlenecks, we employ a two-stage curriculum: (1) train a deterministic autoencoder to convergence with the KL term disabled, then (2) enable KL regularization and fine-tune as a VAE. This approach prevents early posterior collapse and yields stable convergence even at high compression ratios, without increasing total training time.

Computational Cost All experiments were conducted on a single NVIDIA RTX 6000 Ada GPU. Training a $\sim 200M$ parameter VAE at compression ratio $r = 1.6$ requires approximately 1-2 hours for 1B-scale models and 3–4 hours for 7B-scale models ($\sim$500K chunks). Higher compression ratios increase training time proportionally. LoRA weights converge notably faster than full model weights due to their lower-rank structure. At inference, the full encode-decode pipeline completes in 5–10 seconds, enabling rapid iteration during merging experiments.

Reducing the Training Time: Interestingly, in the case of heterogeneous models expansion $r < 1$ can offer an alternative trade-off. Lifting weights into an overcomplete latent space can unfold curved manifolds, making linear interpolation better approximate geodesics on the original weight manifold. expansion forces the encoder to learn a non-trivial transformation, avoiding identity collapse. Practically, expansion significantly accelerates training the relaxed bottleneck eases optimization and improves gradient flow at the cost of increased memory.

C HETEROGENEOUS MODEL MERGING IN LATENT SPACE

Merging models with matched layer shapes is straightforward in weight space. Heterogeneous pairs are harder: to avoid truncating the higher-capacity model, we train *separate* VAEs per architecture and merge in a shared, *aligned* latent space. Concretely, we first calibrate latents per layer, fit an alignment map between the source and target latent spaces, and then interpolate on the target side before decoding. This preserves each model's capacity while enabling stable cross-architecture merges without ad hoc dimensionality cuts. The full procedure is given in Algorithm 2.

Algorithm 2 Details of Heterogeneous LLM Parameter Merging in Latent Space

Require: Source weights W_{src}, target weights W_{tgt}, VAE configs $C_{\text{src}}, C_{\text{tgt}}$
Ensure: Merged weights W_{merged}
1: Initialize VAEs: $(V_{\text{src}}, V_{\text{tgt}}) \leftarrow init(C_{\text{src}}, C_{\text{tgt}})$
2: Load pretrained parameters into $V_{\text{src}}, V_{\text{tgt}}$
3: Split weights into per-layer groups:
$L_{\text{src}} \leftarrow \{\text{all layers from } W_{\text{src}}\}$
$L_{\text{tgt}} \leftarrow \{\text{all layers from } W_{\text{tgt}}\}$
4: Determine the number of pairs to merge: $N \leftarrow \min(|L_{\text{src}}|, |L_{\text{tgt}}|)$
5: Define aligned layer pairs: $(l_{\text{src}}^{(j)}, l_{\text{tgt}}^{(j)})$ for $j = 1, \ldots, N$
6: **for** each aligned pair $(l_{\text{src}}^{(j)}, l_{\text{tgt}}^{(j)})$ **do**
7: Flatten & chunk weights into $\{w_{\text{src}}^{(i)}, w_{\text{tgt}}^{(i)}\}$
8: Encode: $z_{\text{src}}^{(i)} \leftarrow V_{\text{src}}(w_{\text{src}}^{(i)})$, $z_{\text{tgt}}^{(i)} \leftarrow V_{\text{tgt}}(w_{\text{tgt}}^{(i)})$
9: Align latents via OT: $z_{\text{align}}^{(i)} \leftarrow OT(z_{\text{src}}^{(i)}, z_{\text{tgt}}^{(i)})$
10: Merge latents: $z_{\text{merged}}^{(i)} \leftarrow z_{\text{tgt}}^{(i)} + \beta \cdot (z_{\text{align}}^{(i)} - z_{\text{tgt}}^{(i)})$
11: Decode: $w_{\text{merged}}^{(i)} \leftarrow V_{\text{tgt}}^{-1}(z_{\text{merged}}^{(i)})$
12: Store $w_{\text{merged}}^{(i)}$ in W_{merged}
13: **end for**
14: Initialize and evaluate final network with complete W_{merged}
15: **return** W_{merged}

C.1 Intuition Behind Latent Space Alignment

The rationale for restricting explicit latent alignment specifically to heterogeneous merging scenarios relies on the geometric properties of the neural loss landscape and the topological structure of the parameter manifolds.

Homogeneous Merging and Linear Mode Connectivity. In the case of homogeneous models—specifically those finetuned from a shared pretrained initialization (e.g., distinct fine-tunes of LLama-2-13B)—the parameters remain within a shared basin of attraction. Consequently, their weight vectors θ_1, θ_2 reside on a connected region of the high-dimensional parameter manifold $\mathcal{M}$. When encoded into the latent space $\mathcal{Z}$, the resulting distributions $p(z|\theta_1)$ and $p(z|\theta_2)$ naturally share a common support and overlapping density. Therefore, interpolation in $\mathcal{Z}$ corresponds to traversing a flat, low-loss path on the underlying manifold, rendering explicit distributional alignment redundant.

The Heterogeneous Disconnect. Conversely, heterogeneous models (e.g., Gemma-3-1B vs. LLaMA-3.2-1B) possess fundamentally distinct architectures. Even when projected into a latent space of identical dimensionality d, their representations occupy disjoint manifolds $\mathcal{M}_{src}$ and $\mathcal{M}_{tgt}$ with divergent geometric structures and density profiles as show in Figure 9

This disjoint nature necessitates a non-linear mapping to bridge $\mathcal{M}_{src}$ and $\mathcal{M}_{tgt}$. We employ Optimal Transport (specifically the Monge map) to push the source distribution μ_{src} onto the target distribution μ_{tgt} by minimizing the Wasserstein-2 distance. This process essentially "registers" the two manifolds, aligning their statistical moments and geometric structure. By enforcing this alignment, we ensure that the interpolated latent codes z_α remain within the valid density region of the target decoder, thereby preserving functional competence across architectural boundaries.

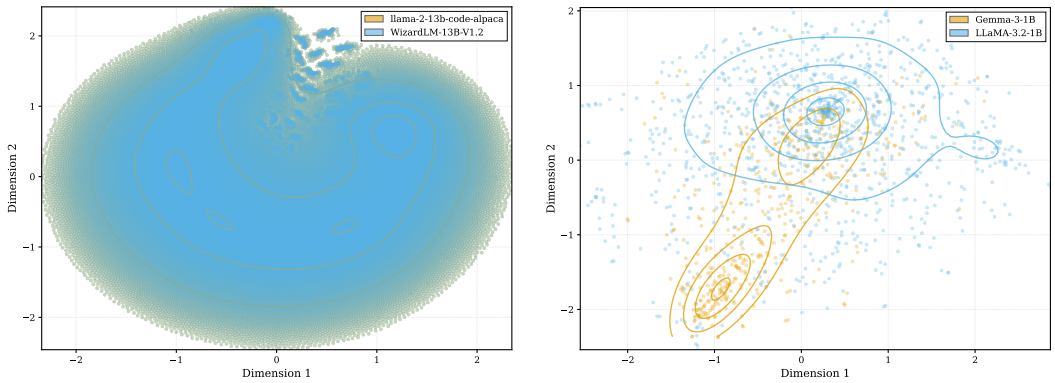

(a) Same-Architecture Fine-tuning Variants: LLaMA-2-13B Code-Alpaca vs WizardLM-13B-V1.2.

(b) Cross-Architecture Comparison: Gemma-3-1B vs LLaMA-3.2-1B.

Figure 9: **VAE latent space reveals architectural signatures in weight distributions.** t-SNE projections of encoded k_proj weights show (**a**) fine-tuned variants of the same base model (LLaMA-2-13B) remain indistinguishable while (**b**) distinct clusters for different architectures (Gemma vs LLaMA) , suggesting the learned latent space captures intrinsic architectural properties.